Published in final edited form as:
Neurobiol Dis. 2012 December ; 48(3): 399–408. doi:10.1016/j.nbd.2012.07.011.

Morphological and functional changes in innervation of a fast forelimb muscle in SOD1-G85R mice

Khanh T. Nguyen[1], **Zhongsheng Zhang**[1], **Ellen F. Barrett**[1,2], and **Gavriel David**[1,2]

[1]Department of Physiology and Biophysics, University of Miami Miller School of Medicine, P.O. Box 016430, Miami FL 33101 USA

[2]Neuroscience Program, University of Miami Miller School of Medicine, P.O. Box 016430, Miami FL 33101 USA

Abstract

Muscle endplates become denervated in mice that express mutations of human superoxide dismutase 1 (hSOD1), models of familial amyotrophic lateral sclerosis. This denervation is especially marked in fast limb muscles, and precedes death of motor neuron somata. This study used mice that expressed yellow fluorescent protein (YFP) in neurons to investigate changes in the morphology and function of axons and motor terminals inervating a fast forelimb muscle (epitrochleoanconeus, ETA) in presymptomatic and symptomatic hSOD1-G85R mice, compared to those in mice that express wild-type (wt) hSOD1. The percentage of endplates (identified using fluorescently-labeled α-bungarotoxin) innervated by motor terminals remained high in presymptomatic SOD1-G85R mice, but fell to ~50% in symptomatic mice. The number of large diameter (≥ 4 μm) axons in the ETA nerve also decreased as mice became symptomatic, and endplate innervation correlated best with the number of large diameter axons. Motor terminal function was assessed using changes in terminal YFP fluorescence evoked by trains of action potentials; different components of the pH-dependent YFP signals reflect stimulation-induced Ca^{2+} entry and vesicular exo/endocytosis. Most visible motor terminals (>90%) remained capable of responding to nerve stimulation in both pre- and symptomatic hSOD1-G85R mice, but with functional alterations. Responses in presymptomatic terminals suggested reduced acidification and increased vesicular release, whereas symptomatic terminals exhibited increased acidification and reduced vesicular release. The fact that most remaining terminals were able to respond to nerve stimulation suggests that motor terminal-protective therapies might contribute to preserving neuromuscular function in fALS mice.

Keywords

familial amyotrophic lateral sclerosis; superoxide dismutase 1 G85R; yellow fluorescent protein; motor nerve terminal; neuromuscular junction; denervation; motor axon; cytosolic pH; calcium; exocytosis

Corresponding author: Gavriel David, Department of Physiology and Biophysics, R-430, University of Miami Miller School of Medicine, 1600 N.W. 10th Ave., Miami, FL, 33136, USA, or, P.O. Box 016430, Miami, FL, 33101, USA, gdavid@med.miami.edu, 305-243-6270 (phone), 305-243-5931 (FAX).

Introduction

Multiple types of mutation in superoxide dismutase 1 (SOD1) produce some familial forms of amyotrophic lateral sclerosis (fALS, Deng et al., 1993). In mice expressing a fALS-inducing SOD1 mutation, one of the earliest signs of disease is degeneration of axons and motor terminals that innervate fast limb muscles (reviewed by Fischer and Glass, 2007; Murray et al., 2010). This degeneration occurs before motor neuron cell bodies degenerate, leading to the suggestion that this disease be classified as a distal axonopathy (Fischer et al., 2004). In hSOD1-G93A mice, the most extensively studied of the fALS-inducing hSOD1 mutations, a scenario involving successive waves of motor axon/terminal degeneration has been proposed for hind limb muscles in which the large diameter motor axons/terminals innervating fast, fatiguable (FF, type IIB) muscles degenerate first (Frey et al., 2000; Pun et al., 2006). Signals from denervated muscles then attract sprouts from still-surviving smaller diameter motor axons/terminals that innervate fast, fatigue-resistant (FR, Type IIA) and slow muscles. The FR motor axons/terminals then degenerate, so that only slow axons/terminals remain able to sprout to fill vacant endplates. Additional studies have yielded results consistent with this scenario. For example,Schaefer et al. (2005) presented evidence that multiple muscles from symptomatic hSOD1-G93A mice contain two distinct population of motor units: one population with multiple degenerating/degenerated terminals, the other with abnormally enlarged motor units with no/few degenerated terminals.

The above scenario predicts that, due to sprouting, most muscle endplates will remain innervated until later stages of the disease, when the remaining slow motor axons either themselves degenerate or reach their limit for innervating extra endplates. Consistent with this scenario, measurements of motor units in mutant hSOD1 mice have confirmed early loss of FF motor units and an early decline in motor unit number, with evidence for replacement of some degenerating FF motor units by FR motor units (Hegedus et al., 2007, 2008). However, these studies have also documented that muscle force and motor unit number begin to decline *together*, suggesting that sprouting of remaining motor neurons is incomplete, or that the newly sprouted motor terminals function poorly and/or provide inadequate trophic support to muscle fibers.

The present study investigated whether the motor terminals that persist in pre- and symptomatic hSOD1-G85R muscles remain functional. We used the epitrochleoanconeus (ETA) muscle in transgenic mice that expressed both an fALS-associated mutation (SOD1-G85R) and yellow fluorescent protein (YFP) in neurons. ETA is a small muscle in the forelimb that is comprised mainly of fast muscle fibers (Rogozhin et al., 2008), and is thin enough to permit visualization of all motor terminals and axons by confocal microscopy. YFP expression in neurons facilitated identification of axons and motor terminals, which were assayed in both presymptomatic and symptomatic hSOD1-G85R mice, and compared with those in mice expressing wild-type (wt) hSOD1. YFP expression also permitted an assay of motor terminal function using pH-dependent changes in YFP fluorescence evoked by repetitive stimulation of the motor nerve. As characterized by Zhang et al. (2010), these flourescence changes yield information related to Ca^{2+} influx into the motor terminal and to vesicular exo/endocytosis. Thus we could investigate whether morphologically detectable motor terminals retain the ability to respond to stimulation, or whether this ability is lost before the motor terminal disappears.

Materials and methods

This study used a mouse model of familial ALS mice, hSOD1-G85R (Tg(SOD1-G85R)148Dwc, founders from Dr. Don Cleveland, University of California San Diego, Bruijn et al., 1997; Ilieva et al., 2008). Control experiments used mice expressing normal

human SOD1 (hSOD1-wt; B6SJL-Tg(SOD1)2Gur/J, founders from Dr. Cleveland). All mice were maintained in the C57BL/6 background for at least 10 generations; hSOD1-G85R and hSOD1-wt mice were housed separately. To facilitate identification of axons and motor terminals, these mice were crossed with mice that express yellow fluorescent protein (YFP) in the cytosol of many neurons (including motor and some sensory neurons), but not in muscle or Schwann cells (B6.Cg-Tg(Thy1-YFP)16Jrs/J, Jackson Labs, Bar Harbor, ME, stock #3709). Ages of presymptomatic hSOD1-G85R mice ranged from 80–220 days; ages of symptomatic mice were 200–392 days, with symptoms defined as absence of hind limb extension, dragging of one or both hind limbs, and/or paralysis of hind limbs or forelimbs. Control hSOD1-wt mice ranged from 264–344 days, and where possible were age-matched with symptomatic hSOD1-G85R mice. Mice were sacrificed using cervical dislocation under deep isoflurane anesthesia (4%), procedures approved by the University of Miami Animal Care and Use Committee.

Experiments used the epitrochleoanconeus (ETA) muscle, a forelimb muscle innervated by a small branch of the radial nerve. The muscle is ~9 mm long. Muscle fibers have a median diameter of 35 μm, and >90% are fast, as determined by immunolabeling with myosin heavy chain and ATPase histochemistry (Bradley et al., 1989; Rhogozhin et al. 2008). There are ~400 total muscle fibers, and an estimated 5–7 motor units, suggesting that a motor unit innervated by one α motor neuron normally includes on average 60–80 muscle fibers. The montage in Fig. 1A shows the entire innervation of ETA, revealed by YFP fluorescence in the innervating motor axons. Assays of endplate occupancy and functional assays based on stimulation-induced changes in YFP fluorescence concentrated on regions at the thinner edges of the muscle; one such region is outlined at the rightmost region of Fig. 1A.

Morphological assays of endplate occupancy used techniques similar to those described in Talbot et al. (2011), as illustrated in Fig. 1B–D. Fluorescently stained muscle endplates, identified by staining with Alexa 594-conjugated α-bungarotoxin (BgTx, Fig. 1C), were imaged with motor axons and terminals identified by transgenically expressed YFP (Fig. 1B). In the pseudocolor overlay image (Fig. 1D), innervated (occupied) endplates appear yellow-orange, and denervated (vacant) endplates appear red. In the wt muscle of Fig. 1D all endplates were innervated; the overlay images in Figs. 2D and 4 show some denervated endplates. Calculations of endplate occupancy were based on assessing at least 30–50 endplates in each muscle.

The number and diameter of axons innervating the ETA muscle were determined using projection images like those in Fig. 1E. Confocal image stacks were collected at 60X (z spacing of 0.1 μm) at the point where the nerve entered the muscle (prior to any intramuscular branching). The diameter of each axon was measured from an internodal region, as the greatest width of that axon identified in the stack (its maximal projection image). Axon numbers were determined from these measurements, as well as from cross sections digitally reconstructed from these projection images (Fig. 1F).

Assays of motor terminal function used stimulation-induced changes in motor terminal YFP fluorescence. For these experiments the ETA muscle was dissected and pinned in a chamber containing physiological saline (in mM) NaCl 137, $NaHCO_3$ 15, KCl 4, $CaCl_2$ 1.8, $MgCl_2$ 1.1, glucose 11.2 and NaH_2PO_4 0.33, aerated with 95% O_2/5% CO_2. Bath pH was maintained at ~7.4. For some records in Fig. 6 buffering was accomplished with 10 mM HEPES instead of HCO_3^-/CO_2. The motor nerve was stimulated at 50 Hz with brief (0.3 ms), suprathreshold depolarizing pulses. Muscle contractions were blocked using 15 μM d-tubocurarine, or by addition of labeled BgTx. Fluorescence changes (ΔF) were normalized to pre-stimulation fluorescence (F_{rest}). These measurements are based on Zhang et al.'s (2010) demonstration that stimulation-induced changes in YFP fluorescence result from pH

changes (increased fluorescence indicates alkalinization) and are Ca^{2+} dependent. Details of the analysis are presented in the descriptions of Figs. 4 and 5 in Results. This YFP-based assay can screen large numbers of motor terminals in a relatively short time, much faster than standard functional assays using electrophysiological measurements of endplate potentials. The YFP-based assay may also be more objective than electrophysiological assays, which might be biased in favor of functional terminals. This bias might arise because it would be hard to determine whether absence of an endplate potential was due to a nonfunctional motor terminal or to failure to impale the muscle fiber sufficiently close to the (unstained) endplate.

Data were analyzed using macros written in IPLabv3.61 (Scanalytics, Inc. Fairfax, VA) and Image J (rsbweb.nih.gov/ij/).

Botulinum toxin A came from BBTech (North Dartmouth, MA); Alexa 594-conjugated α-bungarotoxin from Invitrogen (Carlsbad, CA), other reagents from Sigma-Aldrich.

Statistical tests (described in text and figure legends) were performed using GraphPad Prism (GraphPad Software, La Jolla, CA).

RESULTS

Changes in endplate occupancy and axonal number in ETA of hSOD1-G85R mice

Fig. 2 illustrates the reduction in endplate occupancy and average axonal diameter encountered in the ETA of a symptomatic hSOD1-G85R mouse. The montage of YFP fluorescence in Fig. 2A reveals fewer large axons than in the wt motor nerve of Fig. 1. Expanded views show normal-looking BgTx-labeled endplates (Fig. 2C), but a reduced number of motor terminals (YFP in Fig. 2B, overlay in Fig. 2D). The 5 confocal sections in Fig. 2E show the YFP fluorescence of axons in the nerve trunk entering the muscle; arrows indicate which axons were in best focus in each section. Only 2 large-diameter axons remained. The 8 smaller axons were too small to image reliably with digitally reconstructed images like those in Fig. 1F, but could be traced in serial longitudinal sections. The reconstructed course of each axon is shown in the lower right image in Fig. 2E.

Fig. 3A compares average endplate occupancy in ETA muscles from all analyzed hSOD1-wt and pre- and symptomatic hSOD1-G85R mice. The upper plot in Fig. 3E shows occupancy for individual mice vs. age. All endplates were occupied in hSOD1-wt muscles, and almost all were occupied in presymptomatic hSOD1-G85R muscles as well. Average endplate occupancy fell to ~50% in symptomatic hSOD1-G85R. This major decline is consistent with the fact that ETA is composed mainly of fast muscle fibers, which are especially vulnerable in mutant SOD1 fALS mice.

Fig. 3B compares the average number of large (≥ 4 μm) and small (< 4 μm) diameter axons in the nerve trunk entering the ETA muscle. The lower plot in Fig. 3E shows the number of large axons in individual mice vs. age. The average total number of YFP-labeled axons in hSOD1-wt was ~12. Previous studies of ETA innervation have reported 5–7 motor units, based on recordings of surface electromyograms and counts of intramuscular axons, and 2 muscle spindles (Bradley et al., 1989; Rhogozhin et al., 2008). Our total axon counts are in agreement, assuming that each muscle spindle is innervated by 1–2 sensory axons and one γ-motor neuron.

The number of large diameter axons decreased, and the number of small diameter axons increased, as hSOD1-G85R mice became symptomatic. The cumulative histogram in Fig. 3C affirms this shift toward smaller diameter axons. The total number of YFP-labeled axons

(large + small) was increased (from ~12 to ~16) in presymptomatic mice. This conclusion is tentative, however, because in the longitudinal sections used to assess axonal number it is possible that small axons closely adherent to larger axons may have been undercounted in hSOD1-wt nerves. Our results are consistent with the decline in large diameter axons noted in previous studies of different muscles in mutant hSOD1 fALS mice, and with the increase in the number of small diameter axons noted in the ventral root of these mice (Fischer et al., 2005, see Discussion).

To test which aspect of these axonal changes correlated best with the changes in endplate occupancy, we constructed scatter plots of the fraction of occupied endplates (y-axis) vs. the total number of axons, the number of axons with diameters <4 μm, or the number of axons with diameters ≥4 μm (x-axis). We then determined which type of curve yielded the best fit to the data from symptomatic mice. In no case were the data fit well by a straight line. Fig. 3D shows the best fit obtained for any of these pairings, a sigmoidal curve on a plot whose x-axis was the number of axons with diameters ≥4 μm. This analysis suggests that the remaining large axons provided most of the surviving motor terminals in symptomatic mice.

Changes in motor terminal function in ETA of hSOD1-G85R mice

Fig. 4A–D illustrates results from an experiment assaying endplate innervation and motor terminal function in a microscope field from an ETA muscle in a symptomatic hSOD1-G85R mouse. The BgTx-labelled micrograph (Fig. 4A) includes at least 11 complete endplates. The YFP image shows motor terminals innervating these endplates, and in addition shows long thin processes that likely represent axonal sprouts (e.g., arrowhead in Fig. 4B). The overlay of BgTx and YFP fluorescence images indicates that the 8 numbered endplates retained innervation, but the 3 boxed endplates were vacant (Fig. 4C). The 8 numbered traces show the changes in YFP fluorescence evoked in each of the innervated terminals by motor nerve stimulation (50 Hz, 20 s). All innervated terminals except #4 showed a response. In terminals #1–3, 5 and 8 an initial acidification (decrease in YFP fluorescence) was followed by alkalinization. However in terminals #6 and 7 little or no alkalinization followed the initial acidification.

Fig. 4E presents evidence relevant to interpretation of these stimulation-induced changes in YFP fluorescence. Points in black show the response averaged from hSOD1-wt terminals, demonstrating an acidification phase that begins during stimulation, which then gives way to an alkalinization phase that peaks shortly after stimulation ends. Points in blue show that both acidification and alkalinization responses disappeared when Ca^{2+} was removed from the bathing solution. Points in red show that most of the alkalinization response disappeared in botulinum toxin A, which blocks vesicular exocytosis but does not block Ca^{2+} influx into stimulated nerve terminals. These data are similar to those recorded in YFP-filled wt mouse motor terminals by Zhang et al. (2010) and, combined with results of additional studies detailed in that paper, suggest that this Ca^{2+}-dependent acidification is due mainly to accelerated Ca^{2+} extrusion by the plasma membrane Ca^{2+} ATPase, which imports H^+ as it extrudes Ca^{2+}. Thus the acidification response gives evidence for both conduction of axonal action potentials and Ca^{2+} influx into the terminal. The alkalinization phase results from H^+ extrusion from the cytosol mediated by vesicular H^+-ATPase inserted (temporarily) into the plasma membrane during exocytosis. Thus the alkalinization phase provides evidence for vesicular exocytosis. Based on this interpretation, terminals #1–3 and 5–8 in Fig. 4D all exhibited Ca^{2+} influx in response to the train of axonal action potentials, and of these terminals, all except #7 (and possibly #6) evidenced vesicular exocytosis.

Surprisingly, even at symptomatic stages, >90% of visualized motor terminals continued to respond to axonal stimulation. On average, only 6.7% (9/134) of visualized motor terminals in symptomatic hSOD1-G85R mice exhibited no detectable response to stimulation,

compared to 4.8% (9/186) of terminals in presymptomatic hSOD1-G85R mice and 0.88% (2/226) in hSOD1-wt mice. This difference between hSOD1-G85R and hSOD1-wt terminals was significant ($p<0.05$, Chi-square test), as was the Chi-square trend test along the wt-presymptomatic-symptomatic axis.

Fig. 5A–C presents YFP fluorescence changes averaged from terminals of hSOD1-wt (A), presymptomatic (B) and symptomatic (C) hSOD1-G85R mice. The rightmost trace superimposes all 3 of these averaged responses. Figs. 5D,E superimpose the cumulative histograms for the peak acidification and peak alkalinization responses averaged from each type of terminal, measured as indicated by the arrows in Figs. 5A–C. Presymptomatic hSOD1-G85R terminals exhibited, on average, less acidification and more alkalinization than hSOD1-wt terminals. In contrast, symptomatic hSOD1-G85R terminals had on average greater acidification and less alkalinization. If these changes had been due simply to changes in Ca^{2+} influx, one would expect reduced acidification (reflecting reduced Ca^{2+} influx) to be accompanied by reduced alkalinization (reflecting reduced vesicular exocytosis), and increased acidification to be accompanied by increased alkalinization. Thus the fact that changes in acidification were accompanied by the *opposite* direction of change in alkalinization in both presymptomatic and symptomatic hSOD1-G85R mice suggests that these changes were not due solely to changes in Ca^{2+} influx. Other possible mechanisms are considered in the Discussion.

Fig. 5F shows scatter plots of average peak acidification and peak alkalinization as a function of the fraction of occupied endplates for 6 symptomatic hSOD1-G85R mice. There was no significant correlation between acidification and endplate occupancy, but alkalinization clearly increased with endplate occupancy ($R^2 = 0.83$, $p<0.05$ for deviation from a zero slope). This result suggests that disease severity in symptomatic mice manifested as both reduced endplate occupancy and reduced vesicular exocytosis. The lack of correlation between occupancy and acidification suggests that the smaller alkalinization seen in the more severely affected symptomatic mice was not due simply to masking by an extra-large acidification.

Results shown in Fig. 6 suggest that one possible mechanism underlying the increased acidification measured in terminals from symptomatic mice is an impaired ability to handle the acidification associated with a stimulation-induced Ca^{2+} load. Fig. 6A superimposes stimulation-induced YFP fluorescence changes recorded in hSOD1-wt terminals in the normal HCO_3^-/CO_2 buffered saline (bicarb) with responses recorded in the same terminals bathed in saline buffered instead with the synthetic pH buffer HEPES. Figs. 6B,C show similar superimposed plots for presymptomatic and symptomatic hSOD1-G85R terminals. In all cases the acidification response was greater in HEPES, and this increase was especially marked in symptomatic terminals. A likely explanation for the greater acidification in the HEPES solution measured in all terminals is that the absence of HCO_3^- in the bathing solution blocks activity of the Na^+/HCO_3^- cotransporter (NBC), a major mechanism for extruding H^+ from motor terminals (Zhang et al., 2010). With NBC activity blocked, terminals must rely on other mechanisms for extruding H^+ from cytoplasm, such as the Na^+/H^+ exchanger. Removal of the CO_2/HCO_3^- buffering system also inhibits Na^+-dependent Cl^-/HCO_3^- exchange (NDCB) and reduces the pH buffering power of cytosol (reviewed in Chesler, 2003). The markedly greater stimulation-induced acidification in HEPES buffer measured in symptomatic hSOD1-G85R terminals suggests that these terminals have a much greater dependence on CO_2/HCO_3^- to buffer acid loads than hSOD1-wt or presymptomatic hSOD1-G85R terminals.

DISCUSSION

This study investigated both morphological and functional changes in endplate innervation as fALS mice progress from presymptomatic to symptomatic stages of disease. To our knowledge this is the first such study to focus on the ETA forelimb muscle and on the G85R mutation of hSOD1.

The remaining large diameter axons sustain endplate innervation in symptomatic hSOD1-G85R muscles

In the ETA motor nerve the number of YFP-labeled large diameter (≥ 4 μm) axons decreased as hSOD1-G85R mice progressed from presymptomatic to symptomatic stages of disease, and the number of small diameter axons was increased in both presymptomatic and symptomatic hSOD1-G85R. These findings agree with previous studies documenting a decreased number of large axons and an increased number and/or percentage of small axons in both motor nerves and ventral roots of mutant SOD1 rodents and ALS patients (Hanyu et al., 1982, human C6–7 ventral roots; Bradley et al., 1983, human hypoglossal nerve; Atsumi and Miyatake, 1987, human hypoglossal nerve; Lladó et al., 2006, SOD1-G93A rat phrenic nerve). In most cases it was not possible to determine whether the increased percentage/number of small axons resulted from the disappearance of large axons, from shrinkage of formerly large axons and/or from an actual increase in the number of small axons.Fischer et al. (2005) presented evidence for an increased number of small axons that could *not* be attributed simply to shrinkage/disappearance of large axons (their Table 2). Our data in Fig. 3B also suggest an increase (~40%) in the total number of axons innervating ETA in presymptomatic hSOD1-G85R.

It is unclear whether or not small diameter axons contributed to functional innervation of ETA endplates in symptomatic hSOD1-G85R mice. Some large diameter (>4 μm) axons persisted in symptomatic mice, and endplate occupancy correlated significantly with the number of these large axons (Fig. 3D), but not with the number of small diameter axons. This correlation also suggests that the persisting large diameter axons were not entirely sensory.Schaefer et al. (2005) demonstrated the presence of a subpopulation of motoneurons in hSOD1-G93A mice that survive at late disease stages, and partially compensate (by sprouting) for the loss of endplate innervation. Hegedus et al. (2007, 2008) presented evidence that some FF (type IIB) motor units persist; they suggested that the extra activity demands imposed on the remaining FF units might convert them into less-vulnerable FR (type IIA) and type IID/X, allowing them to persist longer, consistent with results of partial denervation in fALS mice (Gordon et al., 2010). Also,Brotherton et al. (2012) demonstrated that in ventral spinal cord of both hSOD1-fALS mice and human ALS patients only a subset of motor neuron somata were stained by an antibody that recognizes misfolded forms of hSOD1; neighboring motor neurons remained unstained. These findings support the possibility that the majority of the substantial endplate innervation remaining in symptomatic hSOD1-G85R originated from the remaining large motor axons.

Motor terminals in presymptomatic and symptomatic hSOD1-G85R mice retain function

Presymptomatic mice—In hindlimb muscles of presymptomatic hSOD1-G93A mice, muscle force and motor unit number decline in parallel, beginning at the same ages (Hegedus et al., 2007). Yet our data in a fast forelimb muscle of presymptomatic hSOD1-G85R mice indicate that ≥ 95% of muscle endplates remain innervated, with motor terminals that remain capable of responding to motor nerve stimulation. It is possible that force measurements made in hindlimb muscles of presymptomatic G93A mice do not apply to forelimb muscles of presymptomatic G85R mice. But if disease mechanisms are similar in G93A and G85R limbs, one possible resolution to the seeming paradox between force and

endplate occupancy measurements might be a mechanism described for another motor neuron disease, hereditary canine spinal muscular atrophy (HCSMA), which is also characterized by reduction in the force generated during tetanic nerve stimulation prior to overt symptoms and massive motor terminal degeneration. In HCSMA Rich et al. (2002a,b) presented evidence that repetitively stimulated terminals were incapable of evoking sustained muscle contraction due to a reduction in vesicular exocytosis (quantal content was smaller, whereas quantal size was unchanged). However, the stimulation-induced YFP fluorescence changes recorded here suggests that this mechanism *cannot* explain the decreased muscle force in presymptomatic mutant hSOD1 mice: reduced vesicular exocytosis would predict a reduced YFP alkalinization response, but Figs. 5B,E show that the average magnitude of the alkalinization response in terminals of presymptomatic mice was *increased* rather than decreased. This evidence for increased vesicular exocytosis during tetanic stimulation might be explained by replacement of degenerating FF motor terminals with FR terminals, which have a larger pool of vesicles available for release by tetanic stimulation (Reid et al., 1999, 2003). Another possibly related finding is Rochel and Robbins' (1988) demonstration that after partial denervation of mouse soleus in wt mice, terminals of the remaining (and expanding) motor units exhibited a transient increase in quantal content.

If terminals in presymptomatic mutant hSOD1 mice are still fully innervated and releasing vesicles, why is muscle force reduced? One possibility is that the vesicular exocytosis from motor terminals that reinnervate denervated endplates is not sufficient to fully stimulate muscle contraction. The alkalinization recorded by the YFP assays of Figs. 4 and 5 gives evidence for vesicular exocytosis, but does not indicate whether the exocytosed vesicles contained normal amounts of transmitter (Zhang et al., 2010). The magnitude of alkalinization also does not indicate whether the vesicular exocytosis was well synchronized with nerve stimulation or included a large asynchronous component, which would be ineffective for activating muscle contraction. Thus the vesicular exocytosis detected as YFP alkalinization does not guarantee normal force generation by the muscle.Tateno et al. (2009) reported that in presymptomatic hSOD1-G93A mice misfolded mutant hSOD1 reduced transport of the acetylcholine-synthesizing enzyme choline acetyltransferase in the axons of spinal motor neurons. Thus one scenario consistent with our data and the force measurements of Hegedus et al. (2007) is: reduced transmitter content in vesicles → reduced net transmitter release from presymptomatic terminals, offsetting the effect of increased vesicular exocytosis → less activation of muscle. Reduced activation of muscle and/or reduced trophic support of muscle by nerve might not only reduce muscle force, but also generate stimuli favoring axonal sprouting, which might help explain the increased number of small diameter axons seen in presymptomatic muscle. However, both the correlation analysis of Fig. 3D and the reduced force measured by Hegedus et al. suggest that such sprouting produces at best only partial functional compensation.

Symptomatic mice—Schaefer et al. (2005) showed that hindlimb muscles of symptomatic hSOD1-G93A mice contain a population of abnormally enlarged motor units. Their morphological analysis did not, however, indicate whether these remaining motor axons and terminals remained capable of action potential conduction and vesicular release. Our measurements of stimulation-induced changes in YFP fluorescence indicate that in symptomatic hSOD1-G85R mice, where average ETA endplate occupancy is reduced to only ~50%, more than 90% of morphologically surviving terminals remained capable of responding to nerve stimulation.

In symptomatic mice the pattern of stimulation-induced pH changes differed from wt, exhibiting increased acidification and reduced alkalinization. In wt terminals the acidification is due mainly to Ca^{2+} efflux via the plasma membrane Ca^{2+}-ATPase, which

admits H^+ as it extrudes Ca^{2+} (Zhang et al., 2010). One possible cause for the increased acidification is thus increased Ca^{2+} entry, but as mentioned in Results, the altered pattern of pH changes in symptomatic mice cannot be explained simply by an increase in Ca^{2+} influx, because this would be expected to increase vesicular release and thus the recorded alkalinization, in contrast to the measured decrease in alkalinization. Attempts investigate this issue by injecting fluorescent Ca^{2+}-sensitive indicators (as in David and Barrett, 2000) into motor axons from symptomatic mice have thus far been unsuccessful due to the paucity of large axons at this stage of the disease. Another possible cause of increased acidification in terminals of symptomatic mice is failure of other Ca^{2+} sequestering or extruding mechanisms (e.g. mitochondrial Ca^{2+} uptake, plasma membrane Na^+/Ca^{2+} exchanger). Much of the Ca^{2+} load that enters wt motor terminals during repetitive stimulation is sequestered temporarily by passive uptake into mitochondria (David and Barrett, 2000, 2003). The transient partial mitochondrial depolarization induced by stimulation is increased in motor terminals of symptomatic hSOD1-G93A and -G85R terminals (Nguyen et al., 2011), and increased mitochondrial depolarization would diminish net mitochondrial Ca^{2+} uptake. This in turn would upregulate other mechanisms for removing Ca^{2+} from the cytosol, such as the plasma membrane Ca^{2+}-ATPase, with its attendant cytosolic acidification.

The increased acidification in symptomatic motor terminals might also be related to reduced ability to buffer/extrude an acid load (Fig. 6). At least two major mechanisms for H^+ extrusion from motor terminals (Na^+/HCO_3^- co-transport, Na^+/H^+ exchange) depend on the transmembrane electrochemical gradient for Na^+. If the metabolism of symptomatic motor terminals is depressed, accumulation of intracellular Na^+ during stimulation might increase, reducing the transmembrane [Na^+] gradient and thereby the activity of the H^+-extruding mechanisms that rely on this gradient. Reduction of the transmembrane [Na^+] gradient would also reduce Ca^{2+} extrusion via the Na^+/Ca^{2+} exchanger, forcing greater reliance on the (acidifying) Ca^{2+}-ATPase for Ca^{2+} extrusion from the cytosol.

A possible correlate of the decreased alkalinization component of the stimulation-induced pH changes measured in symptomatic mice is the reduction in the readily releasable pool of vesicles measured electrophysiologically in early symptomatic hSOD1-G93A mice by Naumenko et al. (2011). A reduction in the releasable pool has also been reported in patients with (sporadic) ALS (Maselli et al., 1993). In symptomatic mice the average magnitude of alkalinization in a particular ETA muscle was correlated with the fraction of occupied endplates. Taken together, our data suggest that motor terminals retain some ability to respond to nerve stimulation almost until the motor terminal disappears.

In summary, this study investigated morphological and functional changes in the innervation of ETA, a predominantly fast forelimb muscle, in hSOD1-G85R mice. Consistent with findings from hSOD1-G93A mice that the large motor axons and terminals innervating fast muscle fibers are especially vulnerable in fALS mice, we found decreases in the number of large diameter axons as hSOD1-G85R mice progressed from presymptomatic to symptomatic disease. Mean endplate occupancy, reduced to ~50% in symptomatic mice, correlated best with the number of remaining large axons (≥ 4 μm diameter), suggesting that much of the remaining innervation originated from a disease-resistant subpopulation of motor neurons/axons, rather than from the abundance of small axons in the hSOD1-G85R motor nerve. Assays of motor terminal function using pH-dependent changes in YFP fluorescence indicated that >90% of visible motor terminals remained capable of responding to nerve stimulation. The patterns of these fluorescence changes were altered in terminals of symptomatic mice in a manner that suggested disruptions of both ion transport and vesicular release. This evidence for preservation of the ability to respond to nerve stimulation in remaining motor terminals of fALS mice increases the likelihood that therapies that support/

enhance motor terminal function might be effective in prolonging life even at late stages of disease.

Acknowledgments

We thank Dr. John Barrett for valuable discussions and help with writing the manuscript, and Doris Nonner for help with genotyping. Supported by grants from the National Institutes of Health (NINDS R01 58888) and the Muscular Dystrophy Association (#112102, 186832).

Abbreviations

fALS	familial amyotrophic lateral sclerosis
FF	fast fatiguable (type IIB) motor unit/muscle fiber
FR	fast, fatigue-resistant (type IIA) motor unit/muscle fiber
HCSMA	hereditary canine spinal muscular atrophy
HEPES	4-(2-hydroxyethyl)-1-piperazineethanesulfonic acid
hSOD1	human superoxide dismutase I
YFP	yellow fluorescent protein
NBC	sodium bicarbonate cotransporter

REFERENCES

Atsumi T, Miyatake T. Morphometry of the degenerative process in the hypoglossal nerves in amyotrophic lateral sclerosis. Acta Neuropathol. 1987; 73:25–31. [PubMed: 3604571]

Bradley SA, Lyons PR, Slater CR. The epitrochleoanconeus muscles (ETA) of the mouse: a useful muscle for the study of motor innervations*in vitro* . J. Physiol. 1989; 415:3P.

Bradley WG, Good P, Rasool CG, Adelman LS. Morphometric and biochemical studies of peripheral nerves in amyotrophic lateral sclerosis. Ann. Neurol. 1983; 14:267–277. [PubMed: 6195954]

Brotherton TE, Li Y, Cooper D, Gearing M, Julien JP, Rothstein JD, Boylan K, Glass JD. Localization of a toxic form of superoxide dismutase 1 protein to pathologically affected tissues in familial ALS. Proc. Natl. Acad. Sci. U.S.A. 2012; 109:5505–5510. [PubMed: 22431618]

Bruijn LI, Becher MW, Lee MK, Anderson KL, Jemkins NA, Copeland NG, et al. ALS-linked SOD1 mutant G85R mediates damage to astrocytes and promotes rapidly progressive disease with SOD1-containing inclusions. Neuron. 1997; 18:327–338. [PubMed: 9052802]

Chesler M. Regulat ion and modulat ion of pH in the brain. Physiol Rev. 2003; 83:1183–1221. [PubMed: 14506304]

David G, Barrett EF. St imulat ion-evoked increases in cytosolic [Ca^{2+}] in mouse motor nerve terminals are limited by mitochondrial uptake and are temperature-dependent. J. Neurosci. 2000; 20:7290–7296. [PubMed: 11007886]

David G, Barrett EF. Mitochondrial Ca^{2+}uptake prevents desynchronizat ion of quantal release and minimizes deplet ion during repet it ive stimulat ion of mouse motor nerve terminals. J. Physiol. 2003; 548:425–438. [PubMed: 12588898]

Deng H-X, Hentati A, Tainer JA, Iqbal Z, Cayabyab A, Hung W-Y, Getzoff ED, Hu P, Herzfeldt B, Roos RP, Warner C, Deng G, Soriano E, Smyth C, Parge JE, Ahmed A, Roses AD, Hallewell RA, Pericak-Vance MA, Siddique T. Amyot rophic lateral sclerosis and structural defects in Cu, Zn superoxide dismutase. Science. 1993; 261:1047–1051. [PubMed: 8351519]

Fischer LR, Culver DG, Tennant P, Davis AA, Wang M, Castellano-Sanchea A, Khan J, Polak MA, Glass JD. Amyotrophic lateral sclerosis is a distal axonopathy: evidence in mice and man. Exp. Neurol. 2004; 185:232–240. [PubMed: 14736504]

Fischer LR, Culver DG, Davis AA, Tennant P, Wang M, Coleman M, Asress S, Adalbert R, Alexander GM, Glass JD. The WldS gene modestly prolongs survival in the SOD1G93A fALS mouse. Neurobiol. Dis. 2005; 19:293–300. [PubMed: 15837585]

Fischer LR, Glass JD. Axonal degeneration in motor neuron disease. Neurodegener. Dis. 2007; 4:431–442. [PubMed: 17934327]

Frey D, Schneider C, Xu L, Borg J, Spooren W, Caroni P. Early and selective loss of neuromuscular synapse subtypes with low sprouting competence in motoneueron diseases. J. Neurosci. 2000; 20:2534–2542. [PubMed: 10729333]

Gordon T, Tyreman N, Li S, Putman CT, Hegedus J. Functional over-load saves motor units in the SOD1-G93A transgenic mouse model of amyotrophic lateral sclerosis. Neurobiol. Dis. 2010; 37:412–422. [PubMed: 19879358]

Hanyu N, Oguchi K, Yanagisawa N, Tsukagoshi H. Degeneration and regeneration of ventral root motor fibers in amyotrophic lateral sclerosis. Morphometric studies of cervical ventral roots. J. Neurol. Sci. 1982; 55:99–115. [PubMed: 7108564]

Hegedus J, Putman CT, Gordon T. Time course of preferential motor unit loss in the SOD1G93A mouse model of amyotrophic lateral sclerosis. Neurobiol. Dis. 2007; 28:154–164. [PubMed: 17766128]

Hegedus J, Putman DT, Tyreman N, Gordon T. Preferential motor unit loss in the SOD1G93A transgenic mouse model of amyotrophic lateral sclerosis. J. Physiol. 2008; 586:3337–3351. [PubMed: 18467368]

Ilieva HS, Yamanaka K, Malkmus S, Kakinohana O, Yaksh T, Marsala M, Cleveland DW. Mutant dynein (Loa) triggers proprioceptive axon loss that extends survival only in the SOD1 ALS model with highest motor neuron death. Proc. Natl. Acad. Sci. U.S.A. 2008; 105:12599–12604. [PubMed: 18719118]

Lladó J, Haenggeli C, Maragakis NJ, Snyder EY, Rothstein JD. Degeneration of respiratory motor neurons in the SOD1 G93A transgenic rat model of ALS. Neurobiol. Dis. 2006; 21:110–118. [PubMed: 16084734]

Maselli RA, Wollman RL, Leung C, Distad B, Palombi S, Richman DP, Salazar-Grueso EF, Roos RP. Neuromuscular transmission in amyotrophic lateral sclerosis. Muscle Nerve. 1993; 16:1193–1203. [PubMed: 8105377]

Murray LM, Talbot K, Gillingwater TH. Review: Neuromuscular synaptic vulnerability in motor neurone disease: amyotrophic lateral sclerosis and spinal muscular atrophy. Neuropathol Applied Neurobiol. 2010; 36:133–156.

Naumenko N, Pollari E, Kurronen A, Giniatullina R, Shakirzyanova A, Magga J, Koistinaho J, Giniatullin R. Gender-specific mechanism of synaptic impairment and its prevention by GCSF in a mouse model of ALS. Front Cell Neurosci. 2011; 5 article 26 (8 pages). Epub Dec 12.

Nguyen KT, Barrett JN, García-Chacón LE, David G, Barrett EF. Repetitive nerve stimulation transiently opens the mitochondrial permeability transition pore in motor nerve terminals of symptomatic mutant SOD1 mice. Neurobiol. Dis. 2011; 42:381–390. [PubMed: 21310237]

Pun S, Santos AF, Saxena S, Xu L, Caroni P. Selective vulnerability and pruning of phasic motoneuron axons in motoneuron disease alleviated by CNTF. Nature Neurosci. 2006; 9:408–419. [PubMed: 16474388]

Reid B, Slater CR, Bewick GS. Synaptic vesicle dynamics in rat fast and slow motor nerve terminals. J. Neurosci. 1999; 19:2511–2521. [PubMed: 10087065]

Reid B, Martinov VN, Njå A, Lømo T, Bewick GS. Activity-dependent plasticity of transmitter release from nerve terminals in rat fast and slow muscles. J. Neurosci. 2003; 23:9340–9348. [PubMed: 14561861]

Rich MM, Waldeck RF, Cork LC, Balice-Gordon RJ, Fyffe RE, Wang X, Cope TC, Pinter MJ. Reduced endplate currents underlie motor unit dysfunction in canine motor neuron disease. J. Neurophysiol. 2002a; 88:3293–3304. [PubMed: 12466447]

Rich MM, Wang X, Cope TC, Pinter MJ. Reduced neuromuscular quantal content with normal synaptic release time course and depression in canine motor neuron disease. J. Neurophysiol. 2002b; 88:3305–3314. [PubMed: 12466448]

Rochel S, Robbins N. Effect of partial denervation and terminal field expansion on neuromuscular transmitter release and nerve terminal structure. J. Neurosci. 1988; 8:332–338. [PubMed: 2892899]

Rogozhin AA, Pang KK, Bukharaeva E, Young C, Slater CR. Recovery of mouse neuromuscular junctions from single and repeated injections of botulinum neurotoxin. A. J. Physiol. 2008; 586:3163–3182.

Schaefer AM, Sanes JR, Lichtman JW. A compensatory subpopulation of motor neurons in a mouse model of amyotrophic lateral sclerosis. J. Comp. Neurol. 2005; 490:209–219. [PubMed: 16082680]

Talbot JD, David G, Barrett EF, Barrett JN. Calcium dependence of damage to mouse motor nerve terminals following oxygen/glucose deprivation. Exp. Neurol. 2012; 234:95–104. [PubMed: 22206924]

Tateno M, Kato S, Sakurai T, Nukina N, Takahashi R, Araki T. Mutant SOD1 impairs axonal transport of choline acetyltransferase and acetylcholine release by sequestering KAP3. Hum. Mol. Genet. 2009; 18:942–955. [PubMed: 19088126]

Zhang Z, Nguyen KT, Barrett EF, David G. Vesicular ATPase inserted into the plasma membrane of motor terminals by exocytosis alkalinizes cytosolic pH and facilitates endocytosis. Neuron. 2010; 68:1097–1108. [PubMed: 21172612]

Highlights

- Innervation of mouse forelimb muscles was assayed by imaging neuronally-expressed YFP
- Symptomatic SOD1-G85R mice lost motor terminals and large-diameter motor axons
- Activation by action potentials was detected as YFP florescence changes in terminals
- >90% of surviving SOD1-G85R motor terminals remained responsive to stimulation

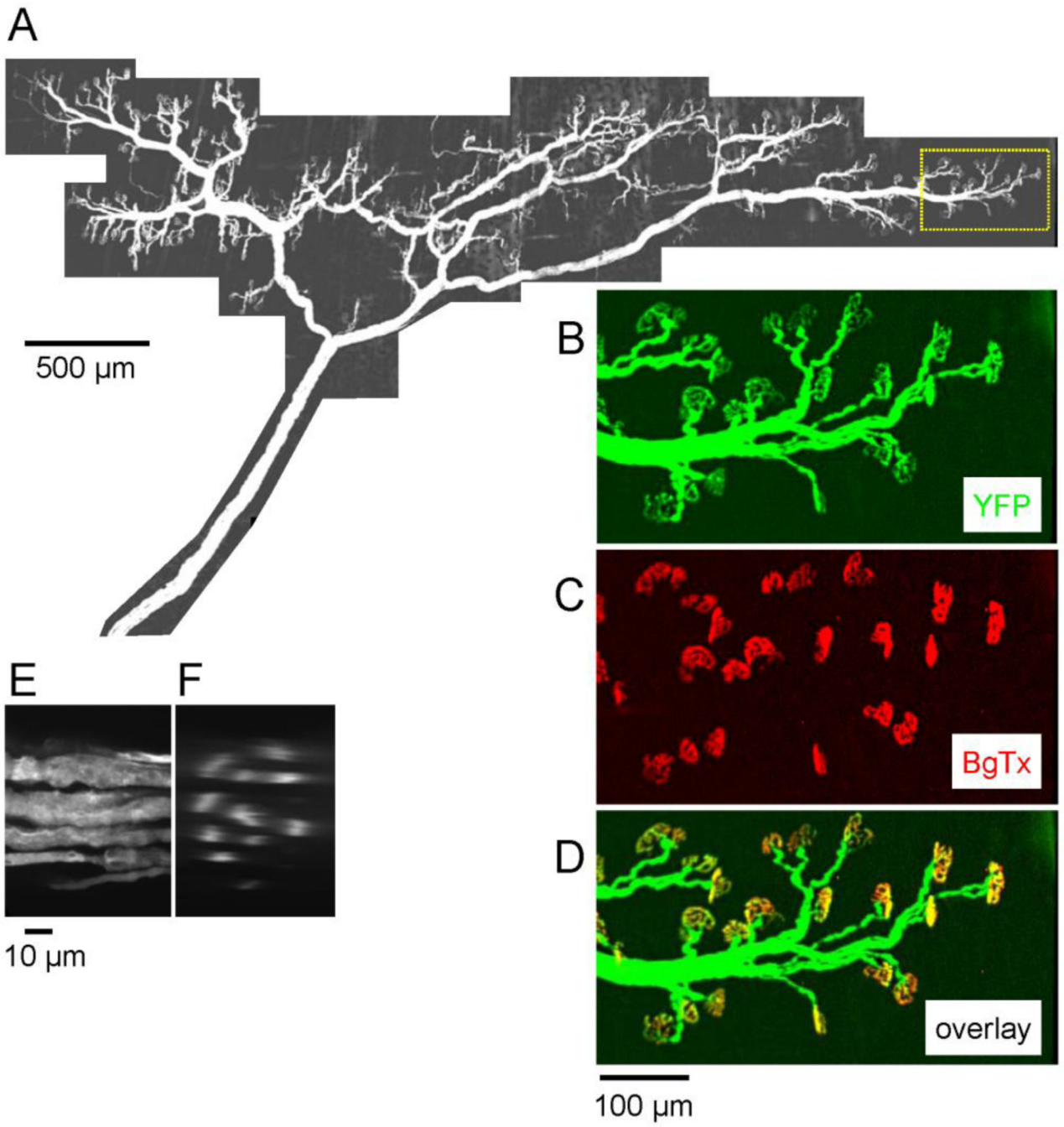

Fig. 1.

Fluorescence micrographs of the motor innervation of the epitrochleoanconeus (ETA) muscle in a mouse expressing YFP in neurons. A. Montage of YFP fluorescence micrographs depicting the complete motor innervation of ETA. Confocal image stacks were acquired with a 10X lens (z spacing = 0.5 µm) at each location and a maximal projection image is shown. The innervation band runs perpendicular to the long axis of the muscle fibers (which are not visible). B–D. Pseudocolored micrographs of the region outlined by dotted lines in A, showing the fluorescence of YFP in green (B) and that of Alexa 594-conjugated α-bungarotoxin (BgTx) in red (C). In the overlay in D, all endplates appear yellow-orange, indicating that each was occupied by a motor terminal. E-F, YFP

fluorescence in the nerve trunk at its entry into the muscle. E is an XY projection image, and F is a reconstructed cross section showing profiles of 11 axons. The projection image in E was assembled from confocal images collected at 60X (z = 0.1 μm). BgTx staining revealed a total of 430 endplates in this muscle; the 407 endplates whose occupancy could be assessed were all completely innervated by a motor terminal. The remaining 23 endplates overlapped the strongly fluorescent nerve trunk, so their occupancy could not be determined.

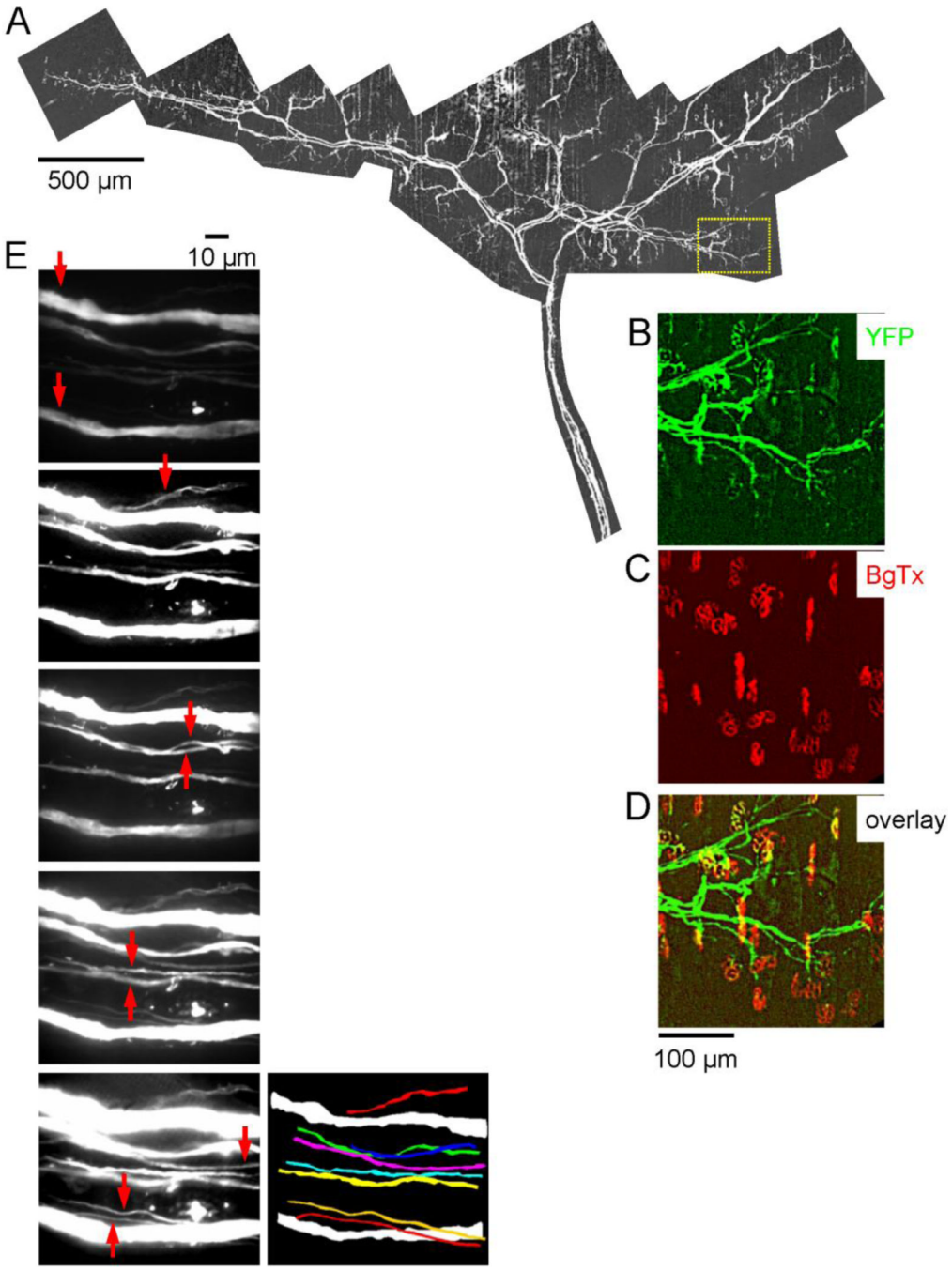

Fig. 2.

Axons and terminals innervating an ETA muscle of a symptomatic hSOD1-G85R mouse. Parts A-D are analogous to their counterparts in Fig. 1. The endplates (C) appear normal, but many are no longer innervated (B,D); in the total muscle 68% (333/489) of endplates were innervated. E, The vertical series of 5 fluorescence micrographs are a subset of XY confocal projection images (60X) showing longitudinal sections through the nerve trunk at its entrance into the muscle. Arrows point to each axon in the section where that axon was best visualized; some thin axons were visible only within a narrow z range. The picture at bottom right is a projection image of all 10 axons, constructed from these sections, with the smaller

axons in color. Only 2 large axons (white) remained. The bright dot located above the lower large axon is likely a remnant of a degenerated axon engulfed by Schwann cells.

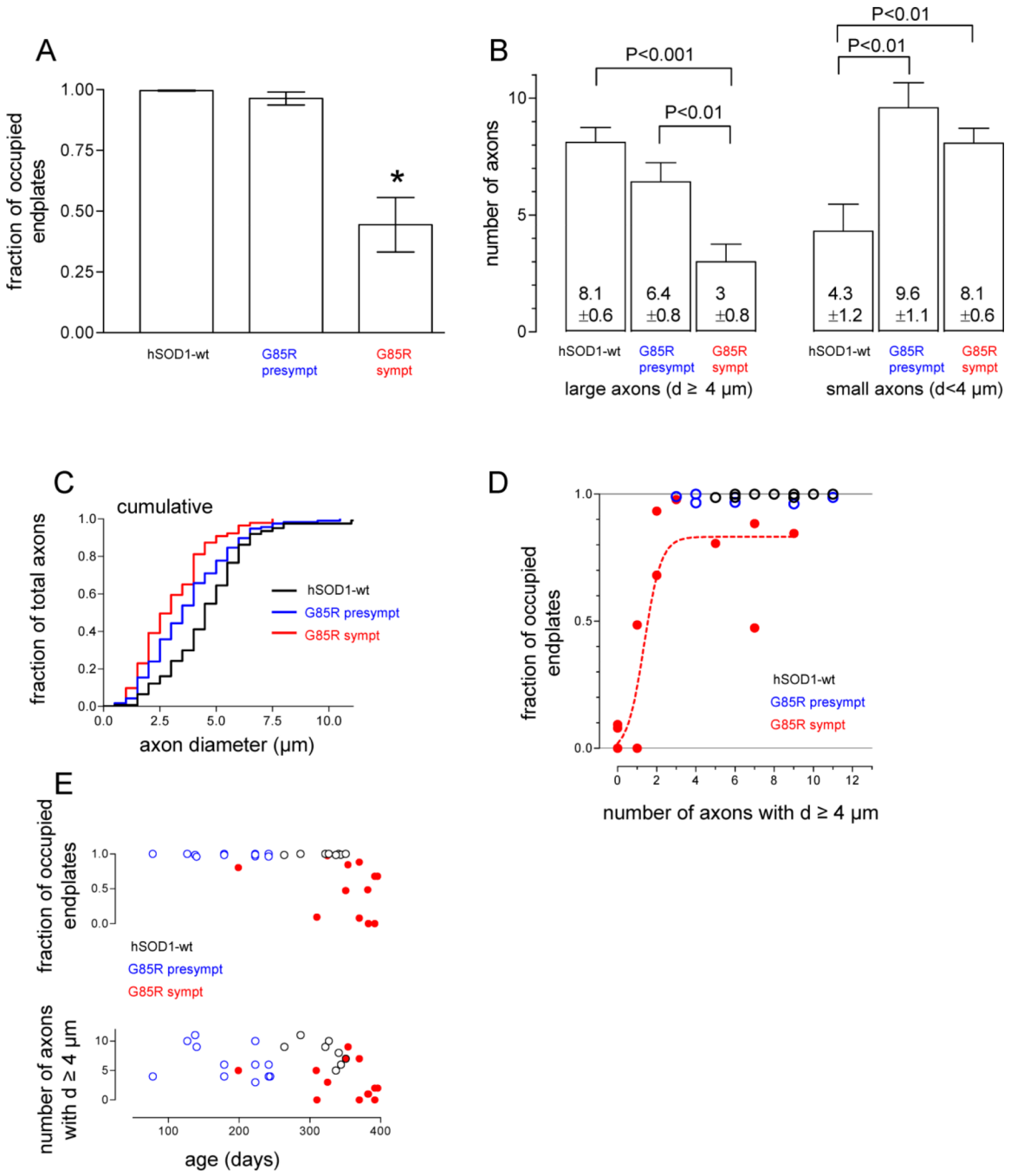

Fig. 3.

Changes in ETA endplate occupancy (A, E) and in the number of large and small diameter ETA motor nerve axons (B, C, E) in presymptomatic and symptomatic hSOD1-G85R mice, and relationship between occupancy and the number of large diameter axons (D). In all panels black = hSOD1-wt, blue = presymptomatic hSOD1-G85R and red = symptomatic hSOD1-G85R. A, Mean fraction of occupied endplates was calculated from 10 wt, 6 presymptomatic G85R and 12 symptomatic G85R mice, with 30–50 BgTx-labelled endplates counted in each muscle. B, Mean number of large (left, diameter ≥ 4 µm) and small (right, diameter < 4 µm) axons, measured from 10 wt, 12 presymptomatic G85R and 15 symptomatic G85R mice; diameters were measured from 124, 117 and 143 axons,

respectively. Means ± SEM. C, superimposed cumulative histograms of axonal diameters for wt, presymptomatic G85R and symptomatic G85R. D, plot of endplate occupancy vs. number of large axons (diameters ≥4 um) for all mice in which both parameters were measured. The sigmoidal curve is the best fit for the symptomatic data ($R^2 = 0.80$). E, age-dependence of fractional endplate occupancy and number of large axons in muscles from animals represented in parts A–D. Each point is measured from one muscle, and measurements from 1–2 muscles are plotted for each animal. Statistical comparisons in A and B used ANOVA followed by Student-Newman-Keuls multiple comparison test (* in A indicates significant difference from wt). Scatter plots like those in D were also prepared with total axon number or number of small axons (diameter <4 μm) on the x-axis; the best sigmoidal fits for these plots had $R^2 = 0.64$ for all axons and $R^2 = 0.11$ for small axons (not shown).

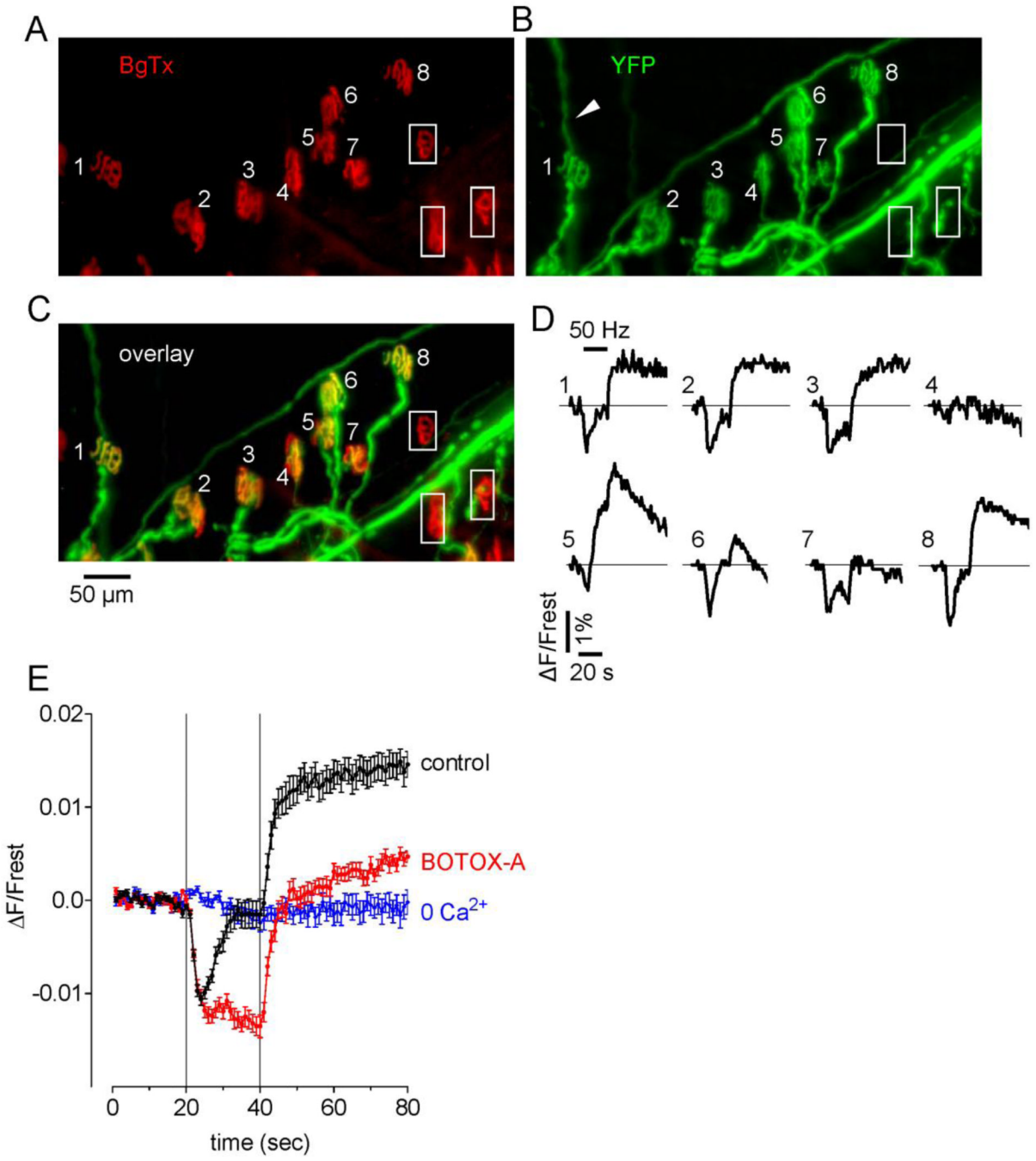

Fig. 4.

Reduced endplate occupancy (A–C) and function (D) at some endplates in a symptomatic hSOD1-G85R mouse, and experiments relevant to interpreting stimulation-induced YFP fluorescence changes (E). A–C, Micrographs show Bg-Tx-labeled endplates (A, red), YFP-labeled motor axon/terminals (B, green) and the overlay of this same microscope field (C). Note the thin YFP-labeled sprouts (e.g., that emanating from terminal #1, arrowhead). The 8 numbered endplates were all innervated; the 3 endplates enclosed in boxes were vacant. D, Traces show stimulation-induced changes in YFP fluorescence recorded at each of the 8 innervated endplates labeled in C (50 Hz, 20 s; horizontal bar over trace 1 indicates the duration of stimulation). E, Superimposed YFP flourescence changes averaged from 10

hSOD1-wt terminals assayed in each of the indicated solutions: physiological saline (control), after addition of botulinum toxin A, and after removal of Ca^{2+} from the bath. Averages are plotted ± SEM. As detailed in Zhang et al. (2010), these data suggest that acidification during stimulation depends on Ca^{2+} influx, and that the subsequent alkalinization following stimulation requires vesicular exocytosis. Thus all terminals except #4, #6 and #7 had both Ca^{2+} influx and vesicular release, terminals #6 and #7 had Ca^{2+} influx but minimal or no vesicular release, and terminal #4 was nonfunctional.

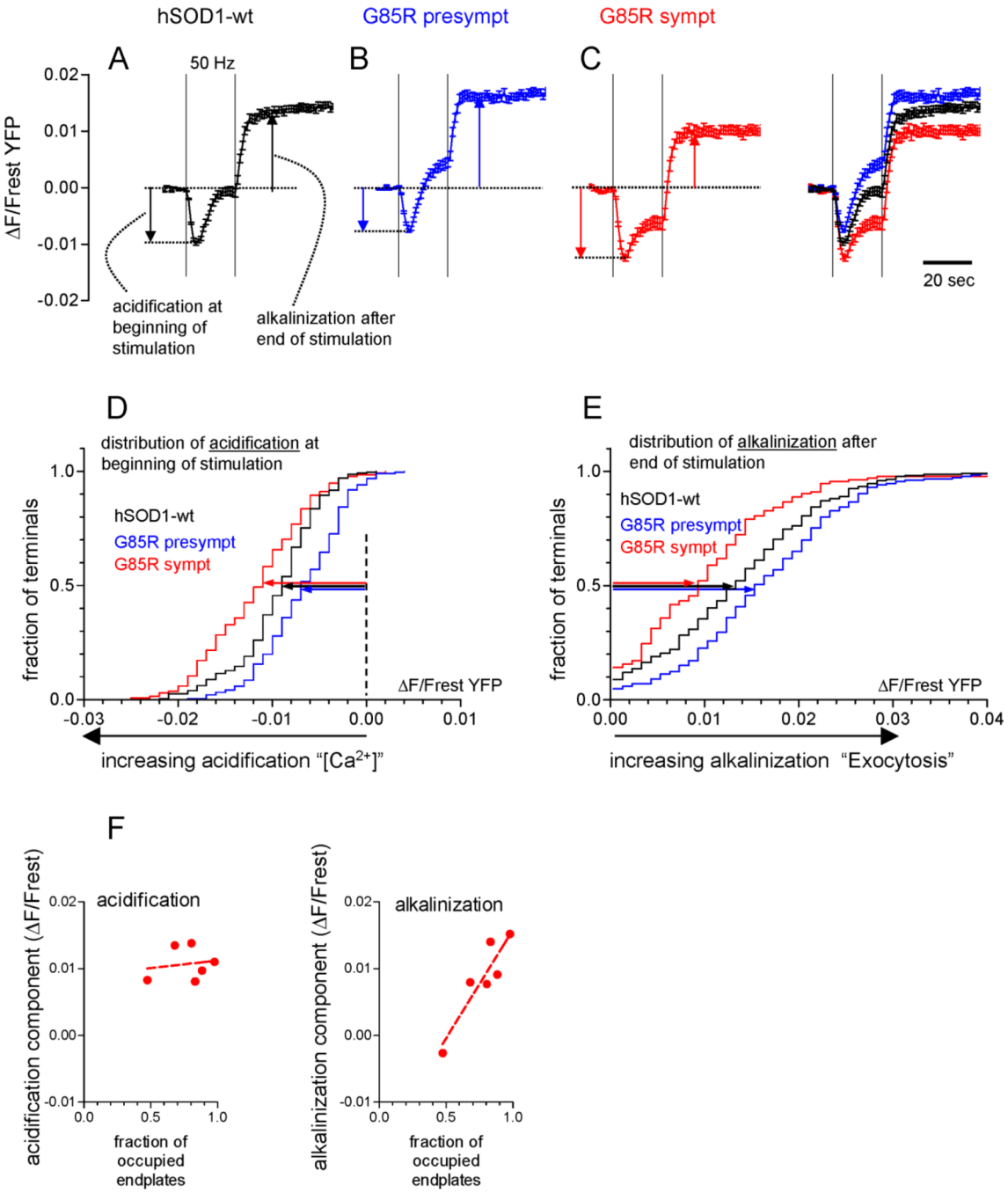

Fig. 5.

Changes in motor terminal function in presymptomatic and symptomatic hSOD1-G85R mice, as revealed by stimulation-induced changes in fluorescence of transgenically-expressed YFP. A–C, Averaged YFP fluorescence changes in response to repetitive nerve stimulation (50 Hz, 20 s) in hSOD1-wt terminals (A) and in presymptomatic (B) and symptomatic (C) hSOD1-G85R terminals. All 3 curves are superimposed at far right. Vertical dashed lines indicate the duration of the stimulus train. As indicated by the vertical arrows, the magnitudes of acidification and post-stimulus alkalinization were measured from the pre-stimulation baseline, justified by the effects of blocking exocytosis with Botox-A in Fig. 4E. Acidification was averaged between the 3rd–6th s of stimulation and alkalinization

was averaged between the 10^{th}–20^{th} s after stimulation ended. D–E, cumulative histograms of acidification from rest and alkalinization from rest, measured as indicated by the arrows in A–C. The length of the horizontal arrows indicates the median magnitude of acidification (D) or alkalinization (E) from rest. These histograms are significantly different from each other at $p<0.01$ or better (Kruskal-Wallis with Dunn's post-test), indicating that presymptomatic hSOD1-G85R terminals acidify less and alkalinize more than hSOD1-wt, and symptomatic hSOD1-G85R acidify more and alkalinize less. Data in A–E are based on measurements from 226 terminals from 5 hSOD1-wt, 186 terminals from 4 presymptomatic hSOD1-G85R, and 134 terminals from 6 symptomatic hSOD1-G85R mice. F, Scatter plots of mean acidification (left) and alkalinization (right) as a function of endplate occupancy; each point represents ETA terminals in 1 of the 6 symptomatic mice that retained some endplate innervation. For acidification $R^2=0.03$; for alkalinization $R^2=0.83$ and $p<0.05$ for deviation from a zero slope. Excluded from the scatter plots in F were data from 3 symptomatic mice whose ETAs exhibited *no* innervated endplates; these muscles had 1, 1 and 0 large-diameter axons and 5, 6 and 4 small-diameter axons, consistent with the idea that small-diameter axons did not contribute to endplate innervation. A similar scatter plot analysis could not be done for presymptomatic mice, because almost all endplates were innervated.

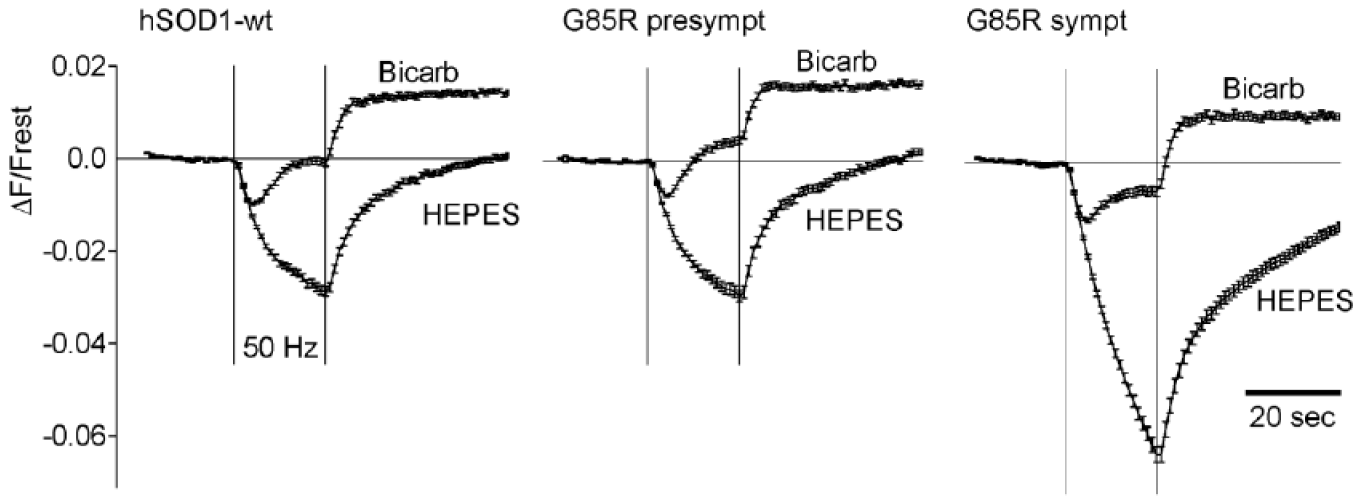

Fig. 6.

Switching from the normal HCO_3^-/CO_2-buffered saline to HEPES-buffered saline alters the pattern of stimulation-induced changes in YFP fluorescence, especially in terminals from symptomatic mice. Each panel superimposes stimulation-induced changes in YFP fluorescence recorded in HCO_3^-/CO_2- and HEPES-buffered saline, averaged for hSOD1-wt, presymptomatic hSOD1-G85R, and symptomatic hSOD1-G85R terminals. All terminals acidified more in HEPES than in bicarbonate buffer; this difference was especially marked in symptomatic hSOD1-G85R terminals. hSOD1-wt data came from 226 terminals in 5 animals (bicarbonate) and 211 terminals in 4 animals (HEPES). Comparable numbers for presymptomatic hSOD1-G85R: 186/4 bicarb, 220/4 HEPES; for symptomatic hSOD1-G85R: 134/6 bicarb, 282/7 HEPES.